

**Electronic Supplementary data**

# **TiO<sub>2</sub> anatase nanorod-decorating for highly efficient photoenergy conversion**

**Dong Hoe Kim,<sup>a</sup> Won Mo Seong,<sup>a,b</sup> Ik Jae Park,<sup>a</sup> Eun- Sang Yu,<sup>c</sup> Seong Sik Shin,<sup>a,b</sup> Ju Seong Kim,<sup>a,b</sup> Hyun Suk Jung,<sup>c</sup> Sangwook Lee,<sup>\*d</sup> and Kug Sun Hong<sup>\*a,b</sup>**

<sup>a</sup>Department of Materials Science and Engineering, Seoul National University, Seoul 151-744, Korea.

<sup>b</sup>WCU Hybrid Materials Program, Department of Materials Science and Engineering, Seoul National University, Seoul 151-744, Korea

<sup>c</sup>School of Advanced Materials Science & Engineering, Sungkyunkwan University, Suwon 440-746, Korea.

<sup>d</sup>Department of Materials Science and Engineering, University of California at Berkeley, CA 94709, USA.

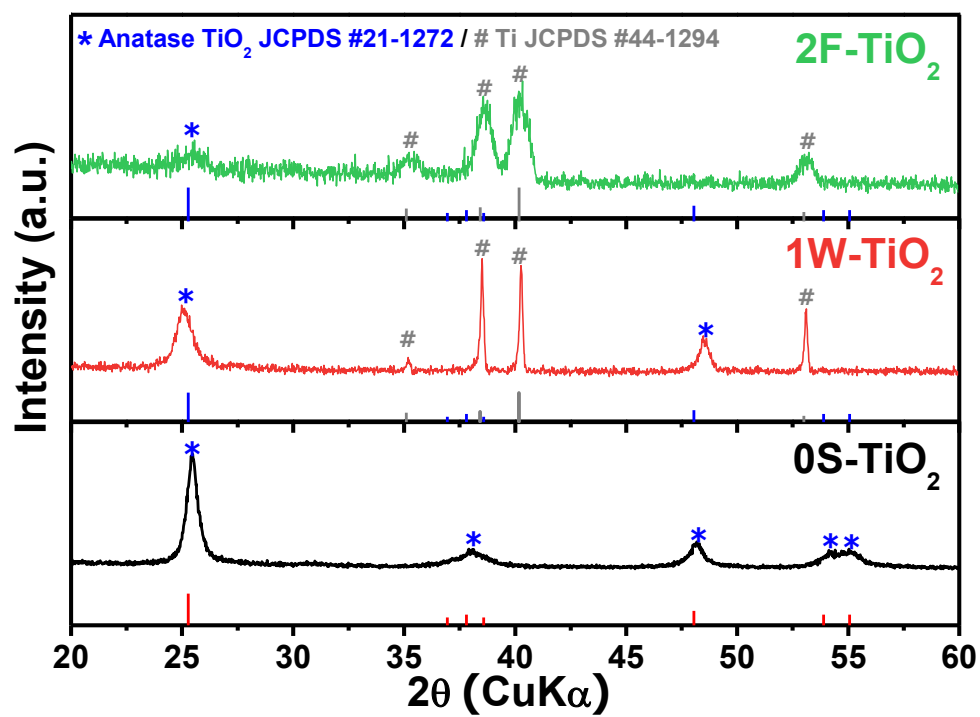


**Fig. S1** XRD patterns of three types  $\text{TiO}_2$  hosts; 0-D sphere  $\text{TiO}_2$  (0S), 1-D wire  $\text{TiO}_2$  (1W), and 2-D thin film  $\text{TiO}_2$  (2F) hosts.

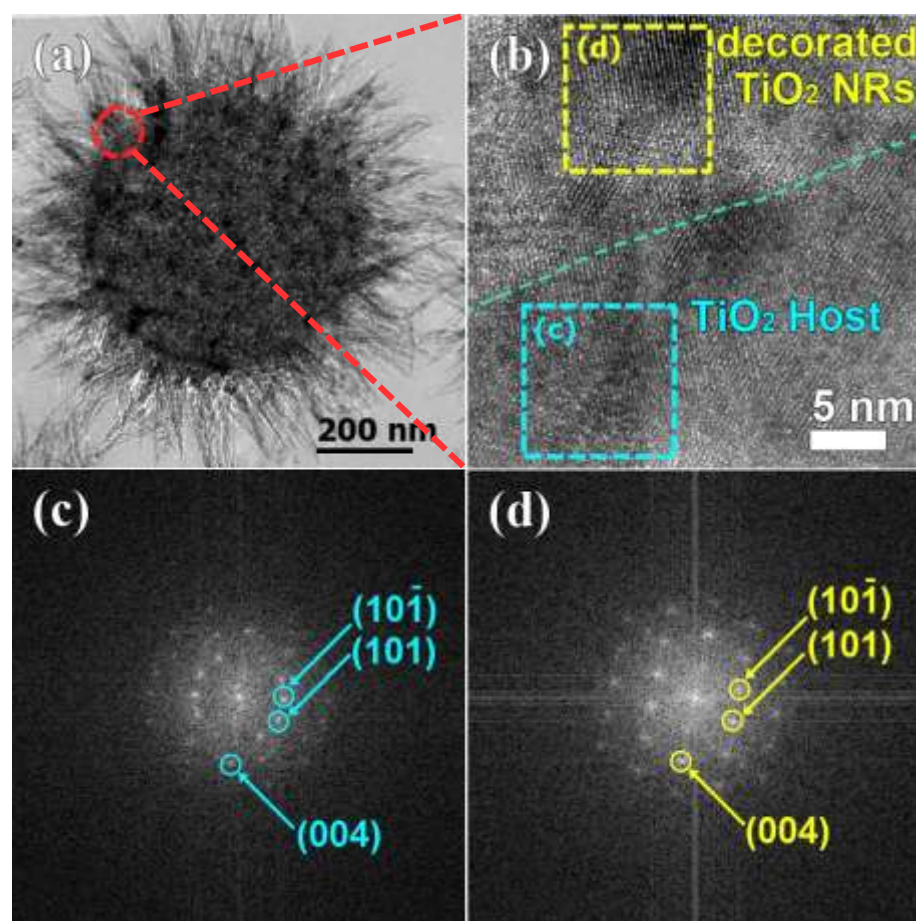


**Fig. S2** (a) Cross-sectional TEM images of BS-TiO<sub>2</sub>, (b) cross-sectional HRTEM images of interface between nanorod branch parts and TiO<sub>2</sub> hosts, and (c), (d) the FFT pattern transformed from the blue and yellow square in (b).

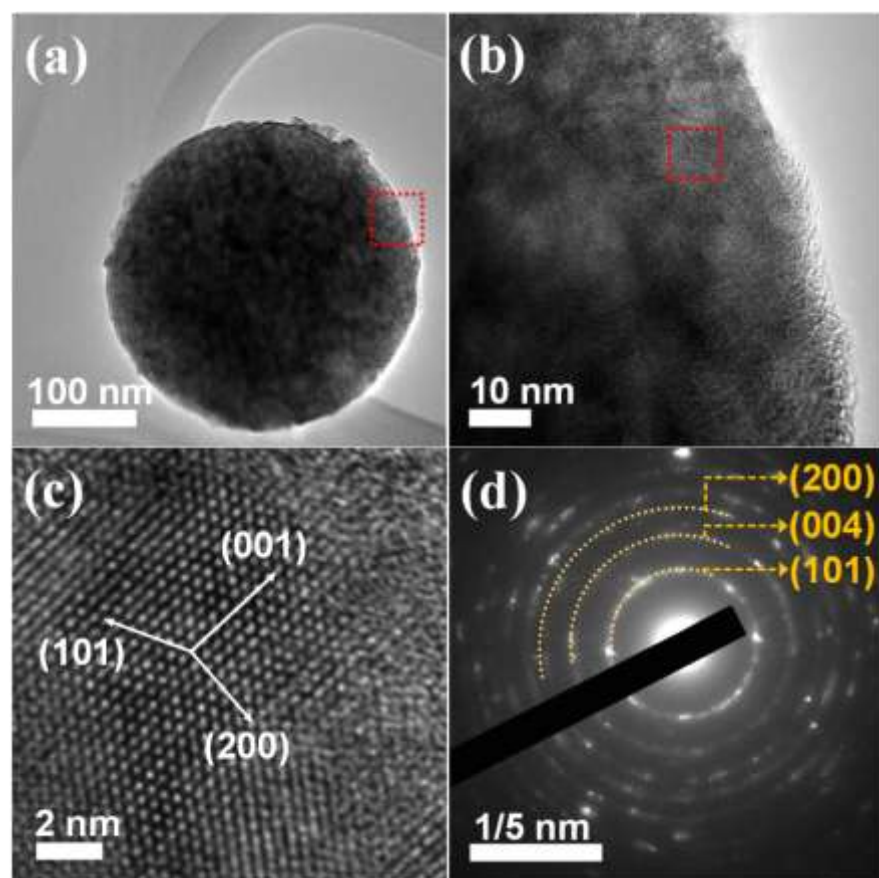


**Fig. S3** (a) Typical TEM images of 0S-TiO<sub>2</sub>, (b) TEM images of surface region of 0S-TiO<sub>2</sub> corresponding with red-dot square in Fig. S3 (a), (c) HRTEM images of nanograins of 0S-TiO<sub>2</sub> corresponding with red-dot square in Fig. S3 (b), and (d) the SAED patterns of one 0S-TiO<sub>2</sub> particle.

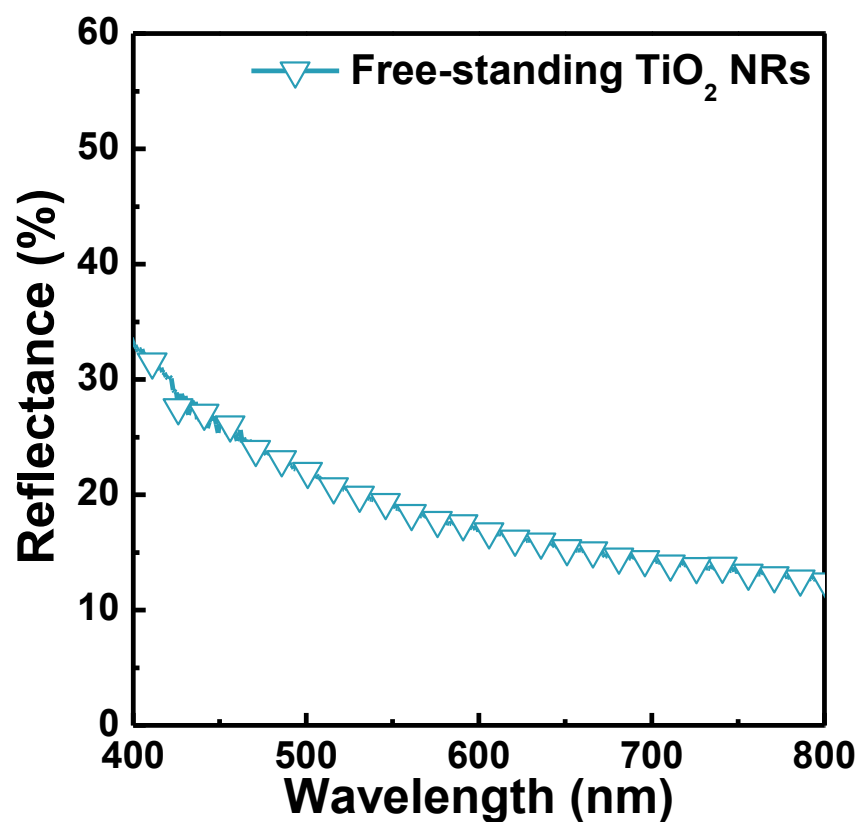


**Fig. S4** Diffused reflectance spectrum of the free-standing  $\text{TiO}_2$  nanorod.

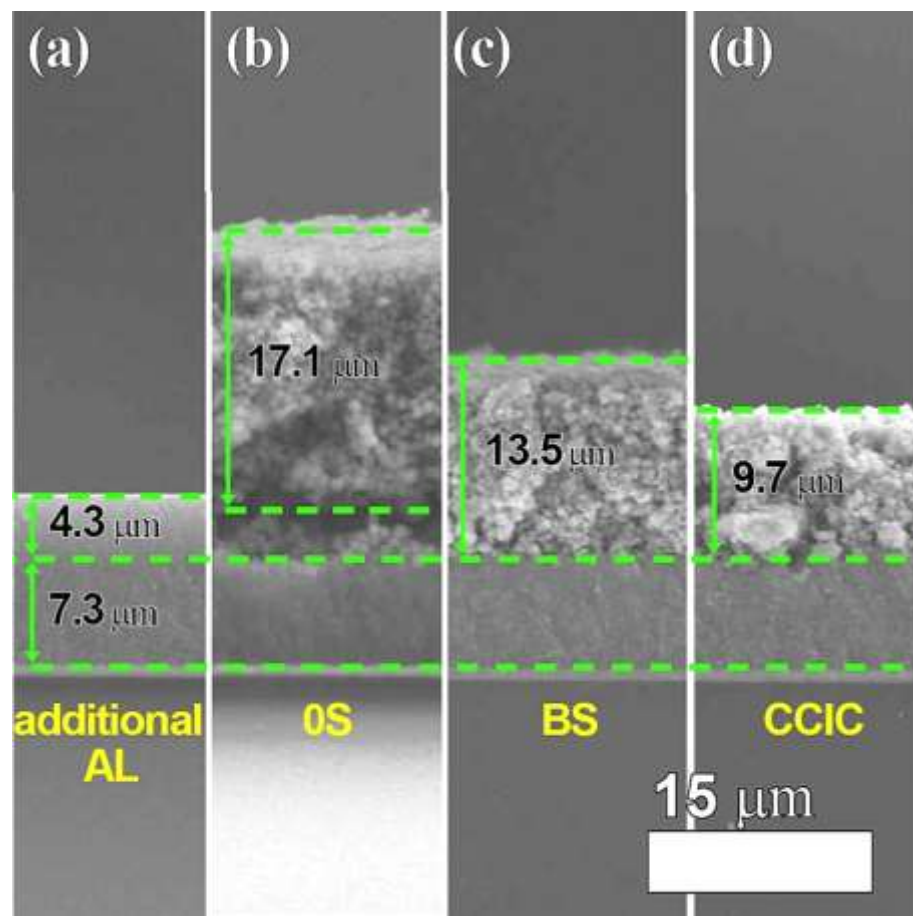


**Fig. S5** Cross-sectional SEM images of photoelectrodes employing various scattering layers with  $t_{\max}$ ; (a) additional AL, (b) 0S, (c) BS, and (d) CCIC.

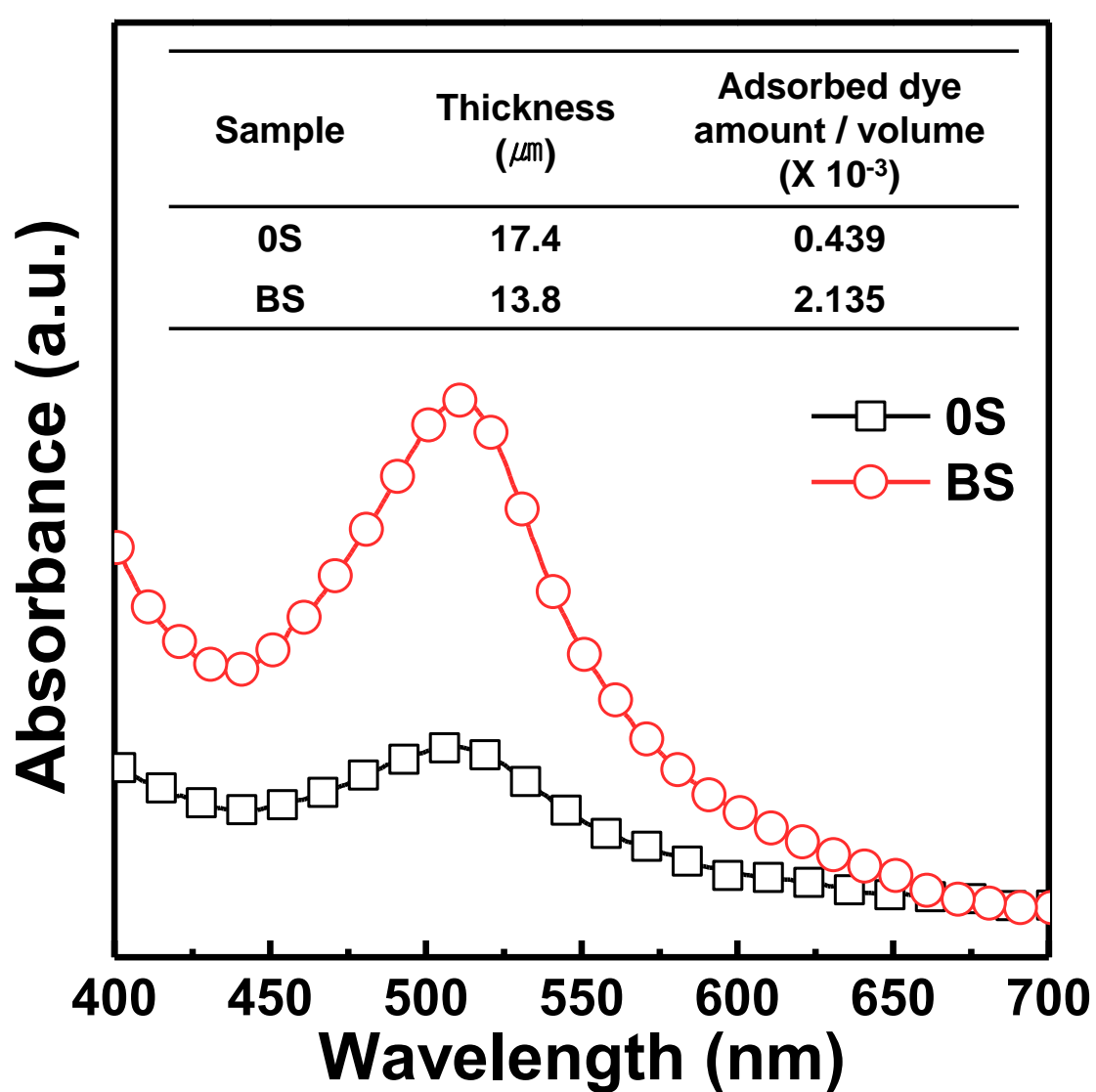


**Fig. S6** The UV-vis absorption spectra of desorbed dye solutions from 0S and BS monolayer films. The inset table shows the thickness of monolayer films and adsorbed dye amount per surface volume.

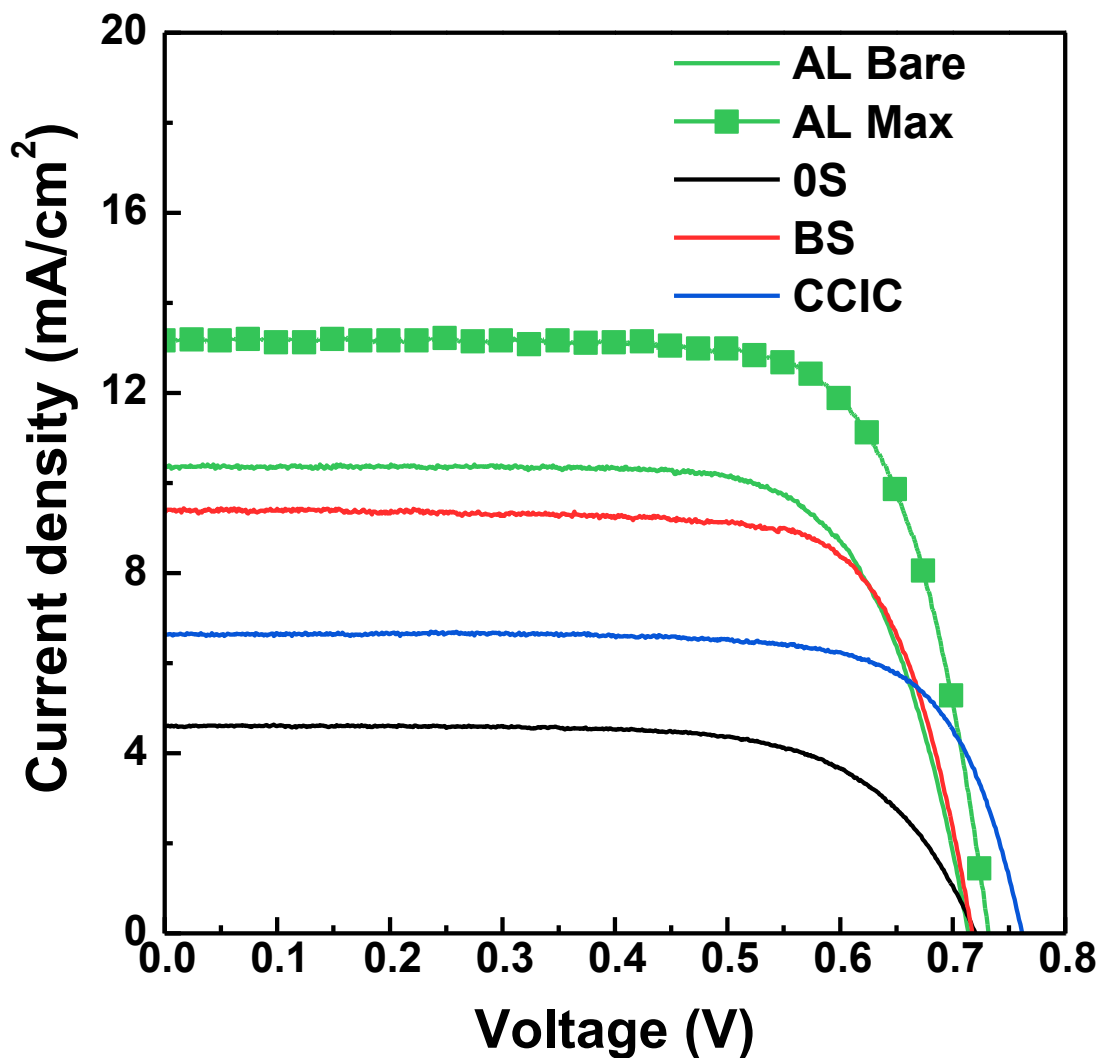
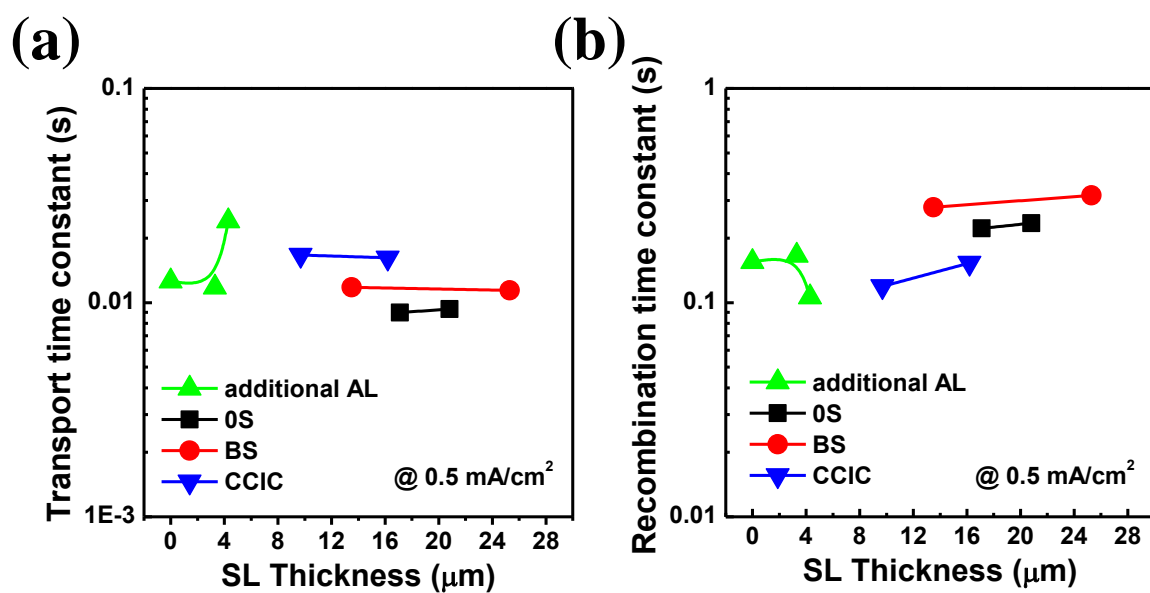


Fig. S7. *J-V* curves of the DSSCs employ each active layer with corresponding certain thickness (AL bare – 7.3 μm, AL Max – 11.6 μm, 0S - 17.4 μm, BS - 13.4 μm, and CCIC - 9.7 μm).



**Fig. S8** (a) Transport time constants and (b) Recombination time constants versus scattering layer thickness of the DSSCs employing each type of scattering layer with various scattering layer thickness at constant photocurrent density ( $J_{\text{sc}} = 0.5 \text{ mA/cm}^2$ ).

**Table S1.** Photovoltaic parameters of the DSSCs employing each type of scattering layer with corresponding  $t_{\max}$  that corresponding with Fig. 5b.

Sample	Thickness ( $\mu\text{m}$ )	$J_{\text{sc}}$ (mA/cm $^2$ )	$V_{\text{oc}}$ (mV)	FF	Efficiency (%)
Additional AL	7.3/4.3	13.2	732	0.74	7.16
0S	7.3/17.1	14.5	732	0.72	7.67
BS	7.3/13.5	17.2	722	0.73	9.09
CCIC	7.3/9.7	15.6	731	0.72	8.26

**Table S2.** Photovoltaic parameters of the DSSCs employing each type of active layer with corresponding certain thickness that corresponding with Fig. S7

<b>Sample</b>	<b>Thickness</b> (μm)	<b><math>J_{sc}</math></b> (mA/cm <sup>2</sup> )	<b><math>V_{oc}</math></b> (mV)	<b>FF</b>	<b>Efficiency</b> (%)
AL Bare	7.3	10.4	715	0.72	5.39
AL Max	11.6	13.2	733	0.74	7.16
0S	17.4	4.61	721	0.69	2.28
BS	13.4	9.39	718	0.75	5.09
CCIC	9.7	6.64	762	0.75	3.80